THE JOURNAL OF BIOLOGICAL CHEMISTRY VOL. 288, NO. 21, pp. 15269–15279, May 24, 2013

Selective Inhibition of Human Group IIA-secreted Phospholipase A_2 (hGIIA) Signaling Reveals Arachidonic Acid Metabolism Is Associated with Colocalization of hGIIA to Vimentin in Rheumatoid Synoviocytes*[S]

Received for publication, Nov. 19, 2012, and in revised form, March 6, 2013 Published, JBC Papers in Press, March 12, 2013, DOI 10.1074/jbc.M112.397893

Lawrence K. Lee,[a,b1] Katherine J. Bryant,[c,d2] Romaric Bouveret,[c,e] Pei-Wen Lei,[c] Anthony P. Duff,[f] Stephen J. Harrop,[g] Edwin P. Huang,[d3] Richard P. Harvey,[c,e] Michael H. Gelb,[h] Peter P. Gray,[d3] Paul M. Curmi,[g,i] Anne M. Cunningham,[j] W. Bret Church,[a,b4] and Kieran F. Scott[c4,5]

From the [a]Faculty of Pharmacy, The University of Sydney, Sydney, New South Wales 2006, Australia, [b]School of Medical Sciences, [c]St. Vincent's Hospital Clinical School, and [j]School of Women's and Children's Health, Faculty of Medicine, [d]Department of Biotechnology, and [g]School of Physics, Faculty of Science, The University of New South Wales, Sydney, New South Wales 2052, Australia, [e]Victor Chang Cardiac Research Institute, Sydney, New South Wales 2010, Australia, [f]The Australian Nuclear Science and Technology Organisation, Sydney, New South Wales 2234, Australia, [i]Centre for Applied Medical Research, St. Vincent's Hospital, Sydney, New South Wales 2010, Australia, and the [h]Departments of Chemistry and Biochemistry, University of Washington, Seattle, Washington 98195

Background: Group IIA secreted phospholipase A_2 (hGIIA) is a bifunctional protein that regulates arachidonic acid metabolism by both catalysis-dependent and catalysis-independent mechanisms.
Results: Selective inhibition of the catalysis-independent signaling function perturbs a hGIIA-vimentin interaction in rheumatoid synoviocytes.
Conclusion: The signaling and catalytic functions of hGIIA are pharmacologically separable.
Significance: Functionally selective inhibitors of hGIIA may provide new avenues for investigation and treatment of immune-mediated inflammation.

Human group IIA secreted phospholipase A_2 (hGIIA) promotes tumor growth and inflammation and can act independently of its well described catalytic lipase activity via an alternative poorly understood signaling pathway. With six chemically diverse inhibitors we show that it is possible to selectively inhibit hGIIA signaling over catalysis, and x-ray crystal structures illustrate that signaling involves a pharmacologically distinct surface to the catalytic site. We demonstrate in rheumatoid fibroblast-like synoviocytes that non-catalytic signaling is associated with rapid internalization of the enzyme and colocalization with vimentin. Trafficking of exogenous hGIIA was monitored with immunofluorescence studies, which revealed that vimentin localization is disrupted by inhibitors of signaling that belong to a rare class of small molecule inhibitors that modulate protein-protein interactions. This study provides structural and pharmacological evidence for an association between vimentin, hGIIA, and arachidonic acid metabolism in synovial inflammation, avenues for selective interrogation of hGIIA signaling, and new strategies for therapeutic hGIIA inhibitor design.

Phospholipase A_2 (PLA_2)[6] enzymes (EC 3.1.1.4) catalyze the hydrolysis of the S_n2 ester bond of glycerophospholipids, thereby regulating the release of biologically active fatty acids and lysophospholipids from membrane phospholipid pools. These lipids are further metabolized within cells to >100 potent autocrine and paracrine lipid mediators. The eicosanoids, which are products of arachidonic acid metabolism by cyclooxygenase, lipoxygenase, and P450 epoxygenase enzymes or by non-enzymatic oxidation, are well recognized modulators of both cell and organ function (1–3). Cell type-specific regulation of the production, concentration, and relative abundance of individual lipid mediators in response to external stimuli serves as an integrated, self-referent, and self-limiting biochemical signaling network in higher organisms. This lipid-signaling network regulates embryonic stem cell dif-

* This work was supported by grants from The National Health and Medical Research Council, The Rebecca Cooper Foundation, the Cancer Council (New South Wales), and the Prostate Cancer Foundation, Australia (to K. F. S.).
[S] This article contains supplemental Figs. 1–5.
The atomic coordinates and structure factors (codes 3U8B, 3U8I, 3U8H, 3U8D) have been deposited in the Protein Data Bank (http://wwpdb.org/).
[1] Present address: Victor Chang Cardiac Research Institute, Lowy Packer Bldg., 405 Liverpool St., Darlinghurst NSW 2010, Australia.
[2] Present address: South West Sydney Clinical School, The University of New South Wales, Liverpool NSW 2170, Australia.
[3] Present address: Australian Institute for Bioengineering and Nanotechnology, Corner College and Cooper Rds. (Bldg. 75), Brisbane QLD 4072 Australia.
[4] Both authors are joint senior authors.
[5] To whom correspondence should be addressed: School of Medicine, The University of Western Sydney. The Ingham Institute of Applied Medical Research, P. O. Box 3151 (Westfields Liverpool) Liverpool, NSW 2170, Australia. Tel.: 61419143647; Fax: 61283471756; E-mail: kieran.scott@unsw.edu.au.

[6] The abbreviations used are: PLA_2, phospholipase A_2; $sPLA_2$, secreted PLA_2; hGIIA, human Group IIA $sPLA_2$; COX-2, cyclooxygenase-2; PGE_2, prostaglandin E_2; FLS, fibroblast-like synoviocyte; BPB, *p*-bromophenacyl bromide; cF, cyclo-(Phe-Leu-Ser-Tyr-Arg); c2, cyclo-((2-Nal)-Leu-Ser-(2-Nal)-Arg).

ferentiation and development and in adult organisms maintains physiological homeostasis in disparate organs such as the gastrointestinal, cardiovascular, renal, reproductive, nervous, and immune systems.

In recent decades manifold PLA_2 proteins with widely divergent selectivity for phospholipid substrate and diverse mechanisms by which their production and enzyme activity are regulated have been discovered in mammals. There are 22 human PLA_2 enzymes that are divided into 15 subgroups defined by structural similarity, catalytic mechanism, calcium requirement, and whether they are secreted (4). This structural and functional diversity within a single enzyme class suggests that the activation and expression of PLA_2 enzymes may be an important control point at which the responsiveness of lipid mediator biosynthesis pathways to external stimuli is regulated and highlights the need for a more detailed understanding of the function and expression of each enzyme.

Aberrant control of eicosanoid signaling contributes to a wide range of human pathological states from headaches to certain cancers. In this context, PLA_2 enzymes have been targeted in the hope that limiting substrate supply rather than selectively blocking the production of particular mediators may be of therapeutic benefit (4). The secreted enzymes ($sPLA_2$s) (5) have been most aggressively targeted thus far. A pan Group IIA/Group V/Group X $sPLA_2$ inhibitor has been tested in clinical trials in sepsis (6), rheumatoid arthritis (7), and coronary artery disease (8) with limited success, likely due to the lack of subtype selectivity of this compound and further highlighting a need for a better understanding of the selectivity of these inhibitors and the function of $sPLA_2$ subtypes in eicosanoid metabolism *in vivo*.

The molecular basis for Group IIA $sPLA_2$ (hGIIA) catalysis is well characterized (5) and can be potently inhibited with substrate analogues or by covalent modification of active site residues. However, recent studies show that hGIIA is a bifunctional protein contributing to arachidonic acid metabolism in cells derived from pathological states by acting both as an enzyme capable of releasing arachidonic acid from microvesicles shed by activated cells and as a catalytic activity-independent indirect amplifier of intracellular eicosanoid production through up-regulation of the cytosolic PLA_2-cyclooxygenase-2 (COX-2) pathway (9). The bifunctional nature of hGIIA in regulating arachidonic acid metabolism raises important questions about the relative contribution of each function to the production of inflammatory mediators and the subsequent promotion of inflammation. Further the findings raise the possibility of selective pharmacological inhibition of each function as a means of investigating the importance of these roles.

Neither the mechanism of hGIIA-mediated signaling nor the relative importance of the signaling function in the promotion of inflammation is known. Here we characterize a chemically diverse set of hGIIA inhibitors in each of two functionally selective assays. We show that there is no correlation between the potency of inhibitors in blocking hGIIA catalysis and their potency in blocking prostaglandin E_2 (PGE_2) production in human rheumatoid fibroblast-like synoviocytes (FLSs), which is a catalytic activity-independent function of hGIIA. Furthermore, we identified three classes of hGIIA inhibitors, those that are (i) selective for catalysis, (ii) non-selective, or (iii) selective for catalysis-independent activity, and determined the crystal structures of hGIIA bound to class (i) and (ii) inhibitors. In combination with the functional assays, these structures indicate that inhibitors of hGIIA signaling in rheumatoid FLS cells operate by perturbing a vimentin binding surface on hGIIA. Finally we demonstrate that the catalysis-independent function of exogenous hGIIA is associated with rapid internalization and colocalization with vimentin in FLSs that is dramatically disrupted by both dual-function and signaling-selective inhibitors but not by catalysis-selective inhibition. Thus, these inhibitors of hGIIA signaling belong to a rare class of small molecule inhibitors that act by modulating protein-protein interactions. The structures also suggest that the signaling and catalytic actions of hGIIA may be mutually exclusive, with transition between the two modes of action regulated by a conformational switch that is unique to the hGIIA subtype involving displacement of His-6. These results provide a solid foundation for the design of further functionally selective inhibitors that will be useful in assessing how the pathophysiology of $sPLA_2$ segregates into its catalytic or non-catalytic actions *in vivo* and in turn the feasibility of developing efficacious $sPLA_2$ inhibitors.

EXPERIMENTAL PROCEDURES

Materials—hGIIA protein was expressed using the stably transfected hGIIA-expressing CHOK1 cell line 5A2 (10) grown on alginate beads and cultivated in a stirred fermenter with a 10-liter working volume. hGIIA was purified and quantified as described previously (10). LY311727 was a gift from Lilly, KH064 was purchased from Sigma, and Me-Indoxam, an indole derivative of the indolizine inhibitor indoxam (11), was synthesized as described (12). The cyclic peptide inhibitors cyclo-FLSYR and cyclo-2-Nal-LS-2-Nal-R were synthesized by Auspep (Melbourne, Australia).

Enzyme Activity Assay—hGIIA catalytic activity was measured with a colorimetric microtiter plate, mixed-micelle assay (13) using diheptanoylthiophosphatidylcholine as substrate (Cayman Chemical, Ann Arbor, MI) as described (9) with the following modifications. Absorbance was read at 405 nm over 70–90 min on a SPECTRAmax 250 microtiter plate spectrophotometer. Statistical data analysis was performed in Microsoft® Excel, and curve fitting and kinetic data analysis were performed using Sigma Plot (SYSTAT, San Jose, CA). Purified hGIIA had a specific activity of 27.8 ± 2.3 μmol of diheptanoylthiophosphatidylcholine/min/mg of protein.

hGIIA Signaling Assay—FLS cells were isolated and cultured from synovial tissue of patients diagnosed with rheumatoid arthritis (14) undergoing joint surgery at St. Vincent's Hospital, Sydney, using procedures approved by the St. Vincent's Hospital Ethics Committee as described (9, 10). Cells (passage 3–10) were plated on 96-well microtiter plates (Greiner), grown to 85–95% confluence, and stimulated for 18 h in serum-free media (DMEM/Ham's F-12 with 0.1% BSA, 200 μl) with 10 ng/ml TNF (20 μl). hGIIA (20 μl, 4 μg/ml) with or without inhibitor was added simultaneously with TNF in inhibitor assays and with various inhibitor concentrations (0.3–10 μg/ml) in dose-response experiments as indicated. Inhibitors (dissolved in DMSO and diluted in serum-free media) were

added (20 μl) where appropriate. Culture medium PGE_2 was quantified by enzyme immunoassay (Cayman Chemical). Cells were detached with 0.05% (w/v) trypsin, 0.53 mM EDTA, and triplicate wells were combined and centrifuged at 8000 $\times$ *g* for 10 min at 4 °C. Cold lysis solution (1% (v/v) Nonidet P-40, 0.5% (w/v) sodium deoxycholate, 0.1% (w/v) SDS, and 1 mM EGTA in PBS with freshly added protease inhibitors 50 μg/ml aprotonin, 200 μM leupeptin, and 1 mM phenylmethylsulfonyl fluoride) was added to the cells and incubated overnight at 4 °C. PGE_2 was normalized for cell count and quantified by measuring total protein in lysates with a detergent-compatible protein assay (Bio-Rad). Independent experiments were performed using cells derived from separate patients.

Crystallization—Pure concentrated hGIIA (5–20 mg/ml) was buffer-exchanged into crystallization buffer containing 0.1 M Tris-HCl, pH 7.4, 10 mM $CaCl_2$, 0.5 mM β-octyl glucoside, and 2 M NaCl precipitate, with 5-kDa Ultrafree-MC Centrifugal Filter Units (Millipore, Billerica, MA). Where appropriate, purified hGIIA (1 mg/ml) was chemically modified with *p*-bromophenacyl bromide (BPB) (Sigma) by coincubation at room temperature overnight with 1 mM BPB in 0.1 M Tris-HCl, pH 8.0, 0.1 M NaCl, and 0.7 mM EDTA. The hGIIA-BPB complex was then exchanged into crystallization buffer containing 0.1 M Tris-HCl, pH 7.4, 10 mM $CaCl_2$, 0.5 mM β-octyl glucoside, and 1 M NaCl, concentrated 10-fold ,then flash-frozen in liquid nitrogen and stored at −80 °C for use in activity assays or crystallization trials.

Crystals were grown by the hanging-drop vapor-diffusion method using 24-well tissue-culture plates (Linbro, ICN Biomedicals). Drops were equilibrated with crystallization buffer with higher NaCl concentrations between 3 and 5 M. Coverslips were purchased pre-siliconized from Hampton Research (Laguna Niguel, CA). 2-μl drops were used in the presence of the inhibitor at approximately 2–5-fold molar excess over protein. Solutions and tissue-culture plates were all stored at crystal growth temperature (293 K) in a Sanyo MIR-2530 incubator (Sanyo Electric) unless otherwise stated. Macroseeding was performed in some instances by immersing nylon loops or human hair into drops containing crushed native crystals then streaking the hair across fresh drops containing enzyme with inhibitor.

Structure Determination—Crystals were mounted onto a nylon loop and flash frozen in liquid nitrogen without cryoprotectant and stored in liquid nitrogen for data collection. X-ray diffraction data were collected ($\Delta\varphi = 0.5°$) at a wavelength of 0.9002 Å with the crystals under a nitrogen stream at 100 K at beamline 14-BMC at the Advanced Photon Source in Chicago on a Area Detector Systems Corporation Quantam-315 charged coupled device detector. Diffraction was indexed and integrated with Denzo and scaled with Scalepack using the HKL-2000 program package (15). Datasets were solved using molecular replacement with either Molrep or Phaser in the CCP4 program suite (16). Coot (17) was used to build and fit models into electron density, and refinement was carried out using Refmac 5.0 in the CCP4 program suite. Models were refined to convergence before waters were added, and inhibitors were not used in rounds of refinement until all identifiable waters were built. The stereochemistry of the structures was assessed using the Molprobity internet server (18). Structures were overlaid using least squares refinement using Lsqkab in the CCP4 program suite. Ray traced images were generated using the PyMOL (19). All $1F_o - 1F_c$ electron density difference maps of inhibitors were generated before building any atoms into the inhibitor density to minimize phase bias. The protein structure data from this publication have been submitted to the Protein Data Bank database and assigned the following accession codes: 3U8B, native hGIIA; 3U8I, hGIIA-BPB complex; 3U8H, hGIIA-KH064 complex; 3U8D, hGIIA-LY311727 complex.

Immunofluorescence and Imaging—When indicated, FLSs (RA61 and RA57; passage 8–13) were treated with hGIIA (2.5 μg/ml) diluted in PBS, 0.1% BSA for 2 min on ice. Cells were then fixed for 2.5 min in 4% paraformaldehyde, 0.1% Triton X-100 for 10 min, blocked for 30 min in blocking solution (0.1% BSA and 10% donkey serum in PBS), and incubated with 4A1 (20) (6 μg/ml), an anti-hGIIA murine monoclonal primary antibody, in blocking solution for 1 h. Cells were washed in PBS and incubated for 30 min in the dark with Alexa Fluor 488 donkey anti-mouse secondary antibody (Invitrogen). After washing, cells were incubated again with 4 μg/ml anti-vimentin antibody (Santa Cruz Biotechnology C-20) in blocking solution for 1 h, washed, and incubated in the dark with Alexa Fluor 555 donkey anti-goat secondary antibody for 30 min. Cells were then mounted in ProLong Gold antifade medium (Invitrogen). Immunofluorescence was collected using laser scanning confocal microscope (Leica TCS SP upright). Images shown are single sections taken from z-stacks acquired using the manufacturer's software. ImageJ (NIH) was used to invert colors, generate merge pictures, and add scale bars. The figure were assembled, and levels were adjusted uniformly using PhotoShop CS4 (Adobe).

RESULTS

Functionally Selective Inhibition of hGIIA—We have previously shown that exogenous addition of hGIIA causes up-regulation of COX-2 expression in FLSs that, on costimulation with the cytokine TNF, causes an increase in PGE_2 production (10). Here we show that covalent modification of the active site His-48 residue with the irreversible inhibitor BPB (21) has no effect on dose-dependent stimulation of PGE_2 production in rheumatoid FLS cells yet completely abrogates enzyme-dependent hydrolysis of diheptanoylthiophosphatidylcholine micelles (Fig. 1, *A* and *B*). Thus, these data together with our similar observations with the activity impaired hGIIA mutant H48Q (9) establish unequivocally that hGIIA stimulation of PGE_2 production and up-regulation of COX-2 occurs independently of its enzyme activity in FLSs. Indeed, two cyclic peptide hGIIA inhibitors (22) appear to selectively inhibit PGE_2 production while being only very weak inhibitors of diheptanoylthiophosphatidylcholine hydrolysis, with maximal inhibition only observed with more than 1×10^6-fold molar excess of peptide (Fig. 1, *C* and *D*). These peptides, cyclo-FLSYR (cF) and the analog cyclo-(2-Nal)-LS-(2-Nal)-R (c2) were derived from residues 70–74 of the primary sequence of hGIIA (22, 23). The ability to selectively inhibit the catalytic and non-catalytic actions of hGIIA establishes that these two functions may be

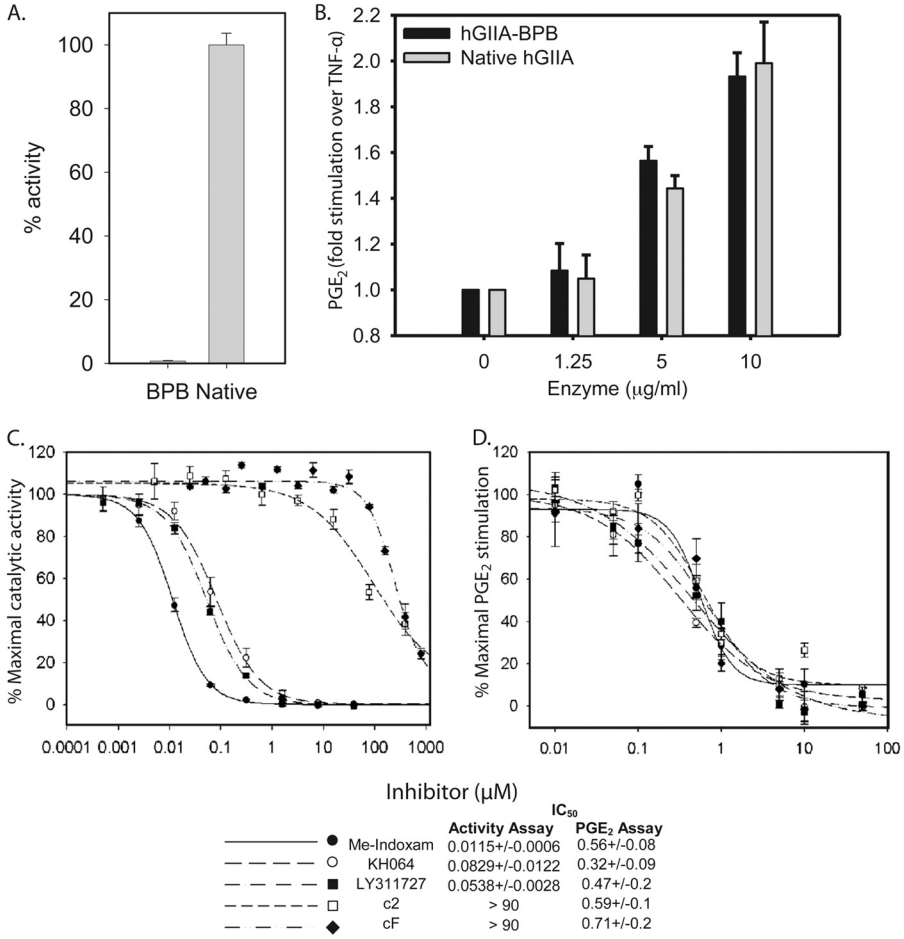

FIGURE 1. **Selective inhibition of hGIIA catalytic activity and signaling.** The effect of BPB modification of hGIIA (BPB in *A* or hGIIA-BPB in *B*) relative to unmodified hGIIA (native in *A* or native hGIIA in *B*) on catalytic activity (*A*) and dose-dependent hGIIA-mediated PGE_2 production (*B*) is shown. *C* and *D* show the dose-dependent effect of non-covalent hGIIA inhibitors on native hGIIA catalytic activity and hGIIA-mediated PGE_2 production, respectively. Catalytic activity was determined using a commercially available mixed-micelle colorimetric assay as described in "Experimental Procedures". The assay was run for 70–90 min, and the initial stable gradient was used to calculate reaction rates. Data (*A* and *C*) are presented as % of uninhibited native hGIIA activity (specific activity, 27.8 ± 2.3 μmol of diheptanoylthiophosphatidylcholine/min/mg or protein) and are the means ± S.E. of 2–3 independent experiments each performed in triplicate with data combined for analysis. PGE_2 production was assessed in cultured FLS cells. Triplicate wells with 90% confluent FLS cells ($n = 5$) in DMEM/Ham's F-12 containing 0.1% BSA were stimulated with TNF (10 ng/ml) together with indicated concentrations of either BPB-modified hGIIA or native hGIIA (*B*). In *panel D*, native hGIIA with inhibitors at the indicated concentrations was added to cells along with TNF. In all cases cells were incubated for 16–20 h. PGE_2 concentrations were determined in triplicate from harvested media using a PGE_2 enzyme-linked immunoassay as described under "Experimental Procedures." Cells were then harvested, and PGE_2 production was normalized for protein concentration of the total cell lysate of three combined wells, as determined by a detergent-compatible protein assay. Data are the mean ± S.E. of 2–5 independent experiments performed in triplicate on primary cells from 2–3 different patients with data combined for analysis.

pharmacologically separated and that inhibition of the signaling function of hGIIA does not depend on direct perturbation of the well characterized His-48—Asp-99 hGIIA catalytic site (5). Finally, the competitive inhibitors Me-Indoxam (12), LY311727 (24), and KH064 (25) dose-dependently inhibited both diheptanoylthiophosphatidylcholine hydrolysis, as well as PGE_2 production in FLSs (Fig. 1, *C* and *D*). However, their relative potency in inhibition of catalytic activity (Me-Indoxam > LY311727 > KH064, spanning an 8-fold range in IC_{50}) appears to be unrelated to their relative potency against cell signaling (KH064 > LY311727 ~ Me-Indoxam, spanning a 2-fold range in IC_{50}). The hGIIA used in these experiments was expressed in mammalian cells; however, lipopolysaccharide (LPS) contamination would nicely explain why BPB-inactivated hGIIA and the H48Q mutant (9) elicit PGE_2 production. Importantly, this LPS hypothesis is ruled out by the fact that both cyclic peptides as well as KH064, LY311727, and Me-Indoxam block hGIIA-dependent PGE_2 production.

As hGIIA signaling is likely mediated by protein-protein interactions rather than by catalysis, inhibitors of signaling probably belong to a relatively rare class of small-molecule inhibitors that operate by disrupting surface protein interactions. To understand how inhibition of hGIIA signaling is mediated and to identify the relevant binding surface and in turn the relevant interacting protein, we determined the crystal structure of the native enzyme in the presence of the active site calcium and in complex with BPB, KH064, and LY311727.

The Crystal Structure of the hGIIA with the Active Site Calcium—Although the structure of the hGIIA without inhibitor bound has been known for well over two decades (26), remarkably there is no native structure modeled with the active site calcium ion bound, which is required for the catalytic activ-

TABLE 1
Data collection and refinement statistics
Values in parentheses are for highest resolution shell.

hGIIA	Native	BPB	KH064	LY311727
Data collection				
Space group	$P6_122$	$P4_1$	$P3_1$	$P3_121$
Cell dimensions				
a, *b*, *c* (Å)	74.7, 74.7, 89.2	70.4, 70.4, 47.3	74.8, 74.8, 49.9	74.4, 74.4, 93.7
σ, β, γ (°)	90.0, 90.0, 120.0	90.0, 90.0, 90.0	90.0, 90.0, 120.0	90.0, 90.0, 120.0
Resolution (Å)	36.7-2.30 (2.42-2.30)	40.0-1.10 (1.16-1.10)	29.9-2.30 (2.42-2.30)	19.8-1.80 (1.90-1.80)
R_{merge}	6.6 (67.0)	13.5 (56.6)	5.5 (24.2)	7.9 (48.2)
Mean $I/\sigma I$	23.0 (4.0)	7.5 (2.1)	11.8 (3.4)	18.3 (3.7)
Completeness (%)	99.3 (99.3)	99.9 (99.9)	97.8 (98.5)	99.9 (98.4)
Redundancy	10.4 (11.1)	4.3 (3.4)	2.8 (2.8)	4.7 (4.5)
Refinement				
Resolution (Å)	24.4-2.3	34.3-1.10	24.8-2.30	19.8-1.80
No. reflections	6,909	91,537	12,907	28,010
R_{work}/R_{free}	20.7/25.7	16.5/18.6	19.2/22.5	12.1/18.9
No. atoms (no H)	1023	2430	2093	2358
Average *B*-factor	66.7	16.6	21.9	20.2
Root mean square deviations				
Bond lengths (Å)	0.018	0.010	0.008	0.016
Bond angles (°)	1.77	1.33	1.10	1.21

TABLE 2
Molprobity structure validation statistics

	Native hGIIA	hGIIA-BPB	hGIIA-KH064	hGIIA-LY311727
Clashscore[a], all atom	4.32	5.42	3.7	6.2
Rotamer outliers	0.00%	0.00%	0.48	0.48
Ramachandran outliers	0.00%	0.00%	0.00%	0.41
Ramachandran favored	97.5%	97.0%	97.13	96.7%
Cβ deviations >0.25Å	0	0	0	0
Overall molprobity score[b]	100th n = 8821 (2.3 ± 0.25 Å)	70th n = 159 (0.09-1 Å)	100th n = 8909 (2.3 ± 0.25 Å)	92nd n = 11,256 (1.8 ± 0.25Å)

[a] Clash score is the number of steric overlaps (>0.4 Å) per 1000 residues.
[b] Values written as percentile where 100th percentile is the best among n structures of comparable resolution (in parentheses).

ity of hGIIA. Furthermore, as mutations in the invariant Gly-30 and the conserved Leu-31 of the calcium binding loop affect $sPLA_2$ binding to its M-type receptor (27), the presence of the calcium may affect the non-catalytic function of hGIIA. To address this, we crystallized hGIIA in similar conditions to those used by Scott *et al.* (28) with 10 mM $CaCl_2$. Hexagonal crystals grew overnight (space group $P6_122$), and diffraction data were collected to 2.26 Å resolution. Diffraction data, refinement, and model validation statistics are summarized in Table 1 and 2. There was a strong density peak in the active site calcium-binding site. The center of the peak was ~2.3 Å from the carbonyl oxygen atoms of His-28, Gly-30, and Gly-32 and the carboxylate moiety of Asp-49 (Fig. 2, *A* and *B*). This typifies the expected stereochemistry of a calcium-binding site. A calcium ion was modeled into the peak and its occupancy refined to 63%, which resulted in minimal residual $1F_o - 1F_c$ difference density. Attempts to refine a fully occupied water molecule in the density peak resulted in significant positive $1F_o - 1F_c$ difference density.

The Structure of the hGIIA-BPB Complex— hGIIA was chemically modified with BPB and crystallized. The crystallographic structure of BPB-inhibited hGIIA was determined from x-ray diffraction data to 1.1 Å resolution from these crystals and has two molecules in the asymmetric unit of a $P4_1$ unit cell. This is the highest resolution crystal structure of any PLA_2 enzyme, and individual atoms are clearly resolvable within the polypeptide chain. Diffraction data, refinement, and model validation statistics are summarized in Tables 1 and 2. BPB is covalently bound to the Nδ of the active site His-48 residue and found wholly within the active site cavity (Fig. 2, *C* and *D*, supplemental Fig. 1). BPB binds in the same way to bovine pancreatic (29) and snake toxin $sPLA_2$ enzymes (30, 31). The phenyl ring on BPB is in contact with Phe-5, Phe-93, and Gly-30 in the hydrophobic active site cavity, and the bromide atom appears to cause a subtle movement in the His-6 side chain away from the active site cavity with the Nδ^1 deviating by ~1.3 Å from the native structure (supplemental Fig. 1). Interestingly the hGIIA-BPB structure retains the active site calcium. This is unique to the BPB-inhibited $sPLA_2$ structures known to date. The calcium ion is coordinated by the carbonyl oxygen atoms of His-28, Gly-30, and Gly-32 on the putative calcium binding loop (28) and a carboxyl oxygen on the Asp-49 side chain. In addition, for the first time, two structural water molecules that coordinate the active site calcium are clearly resolvable. One of these water molecules is on the surface of the enzyme exposed to bulk solvent, and the other (HOH) is in the active site cavity and sterically clashes (2.4 Å) with the carbonyl carbon of BPB (supplemental Fig. 1). Thus, a consequence of the presence of the active site calcium ion in a BPB-modified hGIIA structure is that the active site cavity must be co-occupied by a water molecule and BPB, which forces an apparently energetically unfavorable interaction. This explains both the weaker affinity of calcium for the covalently modified enzyme complex and how mM concentrations of calcium can inhibit BPB modification (21, 32, 33). In addition, the active site calcium shifts away from the inhibitor in the active site cavity by 0.5 Å, and subsequently the coordinating calcium binding loop moves substantially to compensate with Cα deviations up to 2.6 Å. Furthermore, the Asp-49 bidentate coordination to the calcium found in the native structure is disrupted with only one of the Oδ oxygens

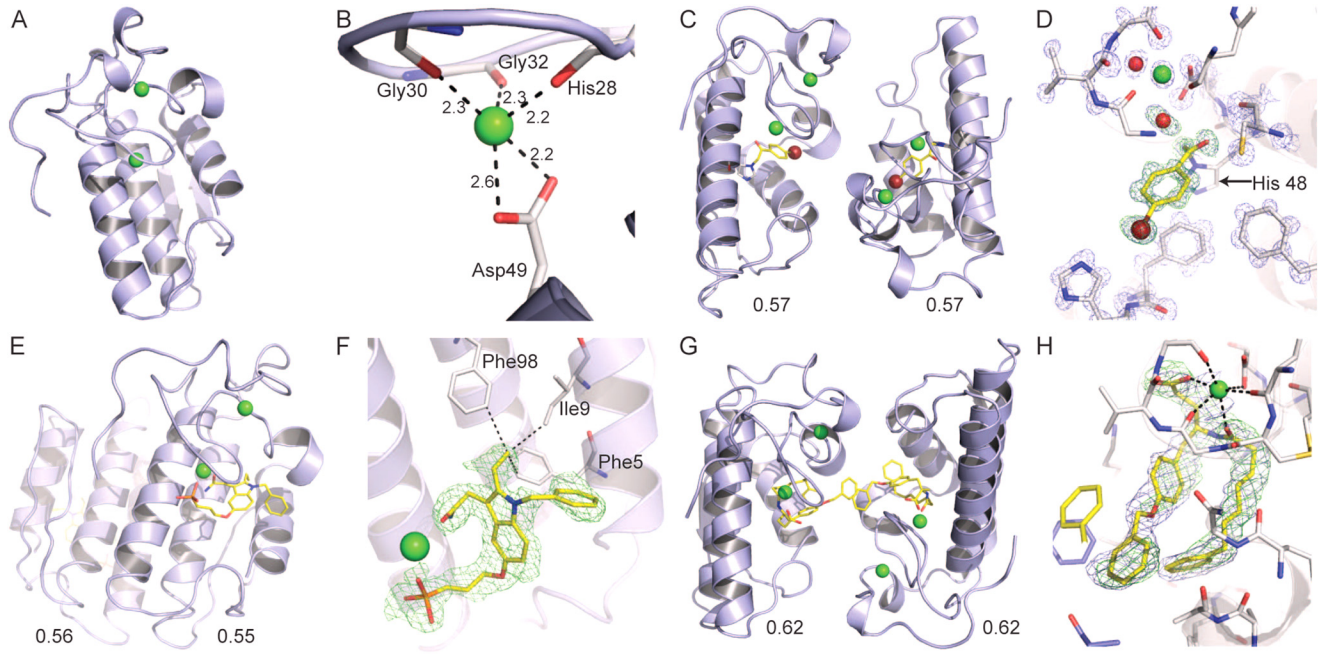

FIGURE 2. **Crystal structures of native and inhibited hGIIA structures.** The asymmetric units of native (*A*), BPB-modified (*C*), LY311727-bound (*E*), and KH064-bound (*G*) hGIIA are rendered in *blue ribbon* format with active site calcium ions shown as *green spheres* and inhibitors shown in *yellow in stick* format. Where applicable, Cα root mean square deviation values from the native structure are shown *underneath their corresponding chains*. *B* depicts the coordination of the active site calcium in the native hGIIA structure. Unbiased $1F_o - 1F_c$ density of BPB (*D*), LY311727 (*F*), and KH064 (*H*) calculated before the inclusion of inhibitors in rounds of refinement are displayed in *green mesh* contoured at 3 σ. Final $2F_o - 1F_c$ density is also contoured at 1.5 σ around selected residues in (D).

coordinating to the calcium and the other hydrogen bonded to HOH.

The Crystal Structure of the hGIIA-LY311727 Complex—The crystals of the hGIIA-LY311727 complex diffracted to 1.8 Å resolution and are primitive hexagonal, belonging to space group $P3_121$. The crystals were twinned with a pseudo-$P6_122$ symmetry. Diffraction data, refinement, and model validation statistics are summarized in Tables 1 and 2. As seen in the structure of hGIIA complexed to indole 8, which differs from LY311727 by a single methyl group (24), a phosphate, and carbonyl oxygen of LY311727, coordinates to the active site calcium and a primary amine makes polar contacts with His-48 and Asp-49 residues (Fig. 2, *E* and *F*). In addition, the hydrophobic indole and phenyl ring makes several hydrophobic interactions along the active site cavity. The additional methyl group on LY311727, absent in indole 8, is buried deep within the hydrophobic cavity and improves the surface complimentarity between the inhibitor and hGIIA. It makes additional hydrophobic contacts with Phe-5, Phe-98, and Ile-9 explaining the 2-fold higher potency of LY311727 in comparison to indole 8 (24) (Fig. 2*F*). Despite their similarities, the hGIIA-LY311727 structure crystallized in a different space group, with two monomers in the asymmetric unit (Fig. 2*E*), suggesting that LY311727 but not indole 8 binding disturbs a crystal contact.

The Crystal Structure of the hGIIA-KH064 Complex—A structure of the hGIIA-KH064 complex was previously reported by Hansford *et al.* (25). However, the inhibitor was modeled in alternate conformations, with steric clashes with the calcium binding loop (PDB accession code 1KQU; supplemental Fig. 2, *A* and *B*). To resolve any ambiguity in the binding mode of KH064, we independently determined the crystal structure of the same complex. As described (25), the hGIIA-KH064 complex crystallized with 2 monomers in the asymmetric unit with inhibitors bound to both monomers (Fig. 2*G*). The structure of the enzyme in each monomer was well preserved with an overall Cα RMS deviation of 0.16 Å. The inhibitor was clearly seen in the active site cavity of both monomers, coordinated to the active site calcium in unbiased $1F_o - 1F_c$ difference electron density, and all regions of both inhibitors were well defined and able to be modeled without ambiguity (Fig. 2*H*). The inhibitor comprises a charged head group and two hydrophobic tails mimicking the S_n1 and S_n2 fatty acid in a glycerophospholipid substrate. The head group and the S_n2 tail of both inhibitors in the asymmetric unit bound to the active site calcium and the hydrophobic cavity, respectively, in a similar fashion. In contrast to the published hGIIA-KH064 structure (PDB code 1KQU), the conformation of the S_n1 tail is not in alternate conformations but in distinct complementary conformations in each monomer that do not clash with the calcium binding loop (Fig. 2*H* and supplemental Fig. 2, *C* and *D*). The phenyl ring extends beyond the active site where it interacts with the equivalent moiety in the second monomer in the asymmetric unit, possibly creating a hydrophobic dimeric interface.

Inhibitors of hGIIA Signaling Perturb Surface Properties without Disrupting the Overall Structure—We compared the structure of native hGIIA containing the active site calcium with the structures of the inactivated H48Q mutant (PDB accession code 1N28 (34)), hGIIA-BPB, hGIIA-LY311727, and hGIIA-KH064. The overall fold of the protein was conserved across all structures, indicating that inhibitors of the signaling function of hGIIA do not induce gross conformational

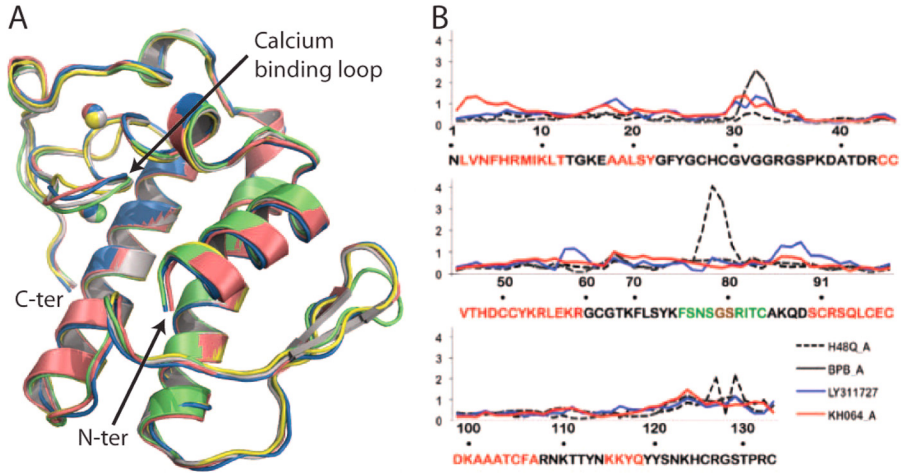

FIGURE 3. **Inhibition of hGIIA activity does not alter its overall structure.** Backbone traces of native hGIIA (*white*), the H48Q mutant (*green*), and when bound to BPB (*yellow*), LY311727 (*blue*), and KH064 (*red*), are overlaid in *A*. Calcium ions are rendered as *spheres*. *B* shows a trace of the Cα root mean square deviations of mutant or inhibited structures from the native enzyme.

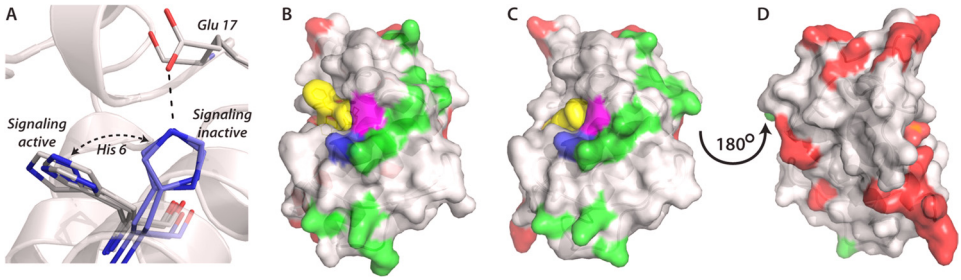

FIGURE 4. **Structural changes induced by inhibitors of hGIIA signaling.** *A*, His-6 is displayed in *white* for signaling active hGIIA structures (native, H48Q mutant, and hGIIA-BPB) and in *blue* for signaling inhibited structures (hGIIA-LY311727 and hGIIA-KH064) The hydrogen bond formed between His-6 and Glu-17 of the hGIIA-LY311727 structures is also labeled. Inhibitors are shown in *yellow*. Arginine and lysine mutations that inhibit or alter hGIIA binding to vimentin are colored in *green* in *B*—*D*, and those that do not inhibit vimentin binding are colored in *red*. The displaced His-6 side chain and the location of the V3W mutation that increases affinity to vimentin are colored in *magenta* and *blue*, respectively, on the hGIIA-KH064 (*B*) and the hGIIA-LY311727 (*C*) complexes. The opposite face of hGIIA-LY311727 is displayed in *panel D*.

changes (Fig. 3). However, inhibitors of hGIIA signaling (KH064 and LY311727), but not the catalytic-selective inhibitor BPB, perturb the surface properties at the entrance to the active site in two ways. First, they displace the His-6 side chain, resulting in the formation of a new hydrogen bond between the His-6 Nδ^1 and the Oδ of Glu-17 (Fig. 4*A*). Second, the His-6 side chain is replaced by a large hydrophobic surface created by phenyl rings of LY311727 and KH064 (Fig. 4, *B* and *C*). This exposed hydrophobic surface spans ~40 Å^2 over the surface of the enzyme for the hGIIA-LY311727 complex and more than 80 Å^2 for the hGIIA-KH064 complex.

The Surface That Is Perturbed by Inhibitors of hGIIA Signaling Correlates to the Vimentin Binding Surface— hGIIA has a large number of solvent-exposed lysine and arginine side chains on the enzyme surface that impart an electropositive coat that is important for heparan sulfate proteoglycan binding (35). Charge reversal of clusters of proximal lysine and arginine residues on the face of hGIIA that includes the entrance to the active site cavity dramatically reduced binding to vimentin, whereas mutations on the opposite side do not (36). In addition, the V3W mutation on the N-terminal helix increased binding to vimentin 3-fold over wild type. Thus, the location of the vimentin binding face correlates with the displaced His-6 side chain and perturbed surface in signaling-inhibited hGIIA structures (Fig. 4, *B*–*D*). These data identify vimentin as a potential binding partner for hGIIA in mediating its signaling function. To test this possibility, we examined the localization of hGIIA when it was added exogenously to FLS cells.

hGIIA Colocalizes with Vimentin— hGIIA was applied to FLS cells grown on coverslips for a short time, and its localization was determined by confocal immunofluorescence microscopy of fixed and permeabilized cells using the hGIIA-specific monoclonal antibody 4A1 (20). The antibody showed negligible staining of cells in the absence of added hGIIA (Fig. 5*A*). On exogenous addition, hGIIA was rapidly internalized by FLS cells and localized in the cytoplasm in filamentous strands with perinuclear staining, with negligible hGIIA detected in the nucleus (Fig. 5*B*). Internalization occurred when cells were preincubated at 4 °C with no obvious effect on the time course, indicating that internalization is likely an energy-independent event. Cells were also stained with anti-vimentin antibodies that showed the well known cytoplasmic and perinuclear staining pattern seen in mesenchymal cells (Fig. 5*C*). In dual immunofluorescence studies, hGIIA colocalized with vimentin (Fig. 5*D*, supplemental Figs. 3 and 4).

Signaling Inhibitors Perturb the hGIIA-Vimentin Interaction— To determine the effect of inhibitors on the hGIIA-vimentin interaction, we repeated the co-immunofluorescence micros-

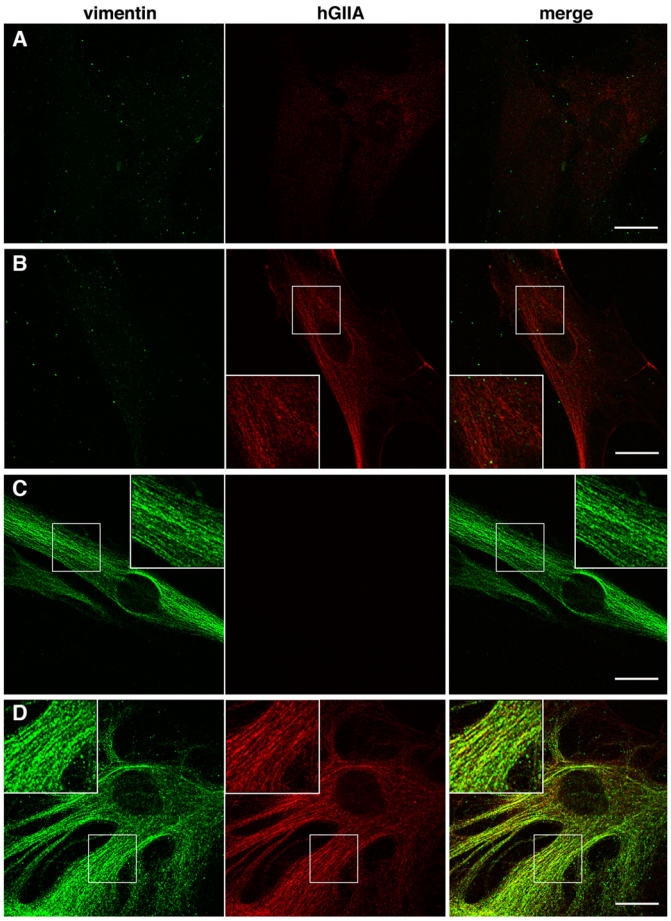

FIGURE 5. **hGIIA internalizes rapidly and co-localizes with vimentin.** Immunofluorescence microscopy on cells stained with anti-hGIIA antibody (4A1 (20)) and/or anti-vimentin antibody. *A*, cells were stained for hGIIA primary antibody alone and subsequently with both 488 and 555 secondary antibodies in the absence of hGIIA treatment and imaged in both 488 nm (hGIIA) and 555 nm (vimentin) channels. Exogenous hGIIA was applied, and cells were stained for hGIIA alone (*B*), vimentin alone (*C*), or hGIIA and vimentin in *D* and imaged as in *A* as described under "Experimental Procedures." Cells were RA61 human rheumatoid FLSs. *Columns 1–3* show vimentin (*green*), hGIIA (*red*), and a merge image, respectively. *Scale bars* represent 20 μm.

copy experiments in the presence of catalysis selective (BPB), signaling-selective (c2 and cF), and non-selective (KH064 and LY311727) inhibitors. Apart from BPB, which becomes covalently bound to the enzyme, inhibitors were incubated with hGIIA before addition to FLSs and dual immunofluorescence labeling. The inhibitors had no observable effect on rapid internalization of hGIIA (Fig. 6, supplemental Fig. 5), and BPB non-modified and modified enzyme colocalized to vimentin (Fig. 6, *A* and *B*, supplemental Fig. 5, *A* and *B*). In contrast, in the presence of KH064, c2, and cF, hGIIA staining was diffuse in the cytoplasm (Fig. 6, *D–F*, supplemental Fig. 5, *D–F*) rather than colocalized with vimentin as seen in the absence of inhibitor (Fig. 6*C*, supplemental Fig. 5*C*). In the presence of LY311727, hGIIA staining was also more diffuse than control; however, some colocalization with vimentin was still observable at the concentration used (*arrowheads* in Fig. 6*G* and supplemental Fig. 5*G*), possibly reflecting differences in the potency of the two compounds in the signaling assay (KH064 > LY311727) relative to the enzyme inhibition assay (Fig. 1).

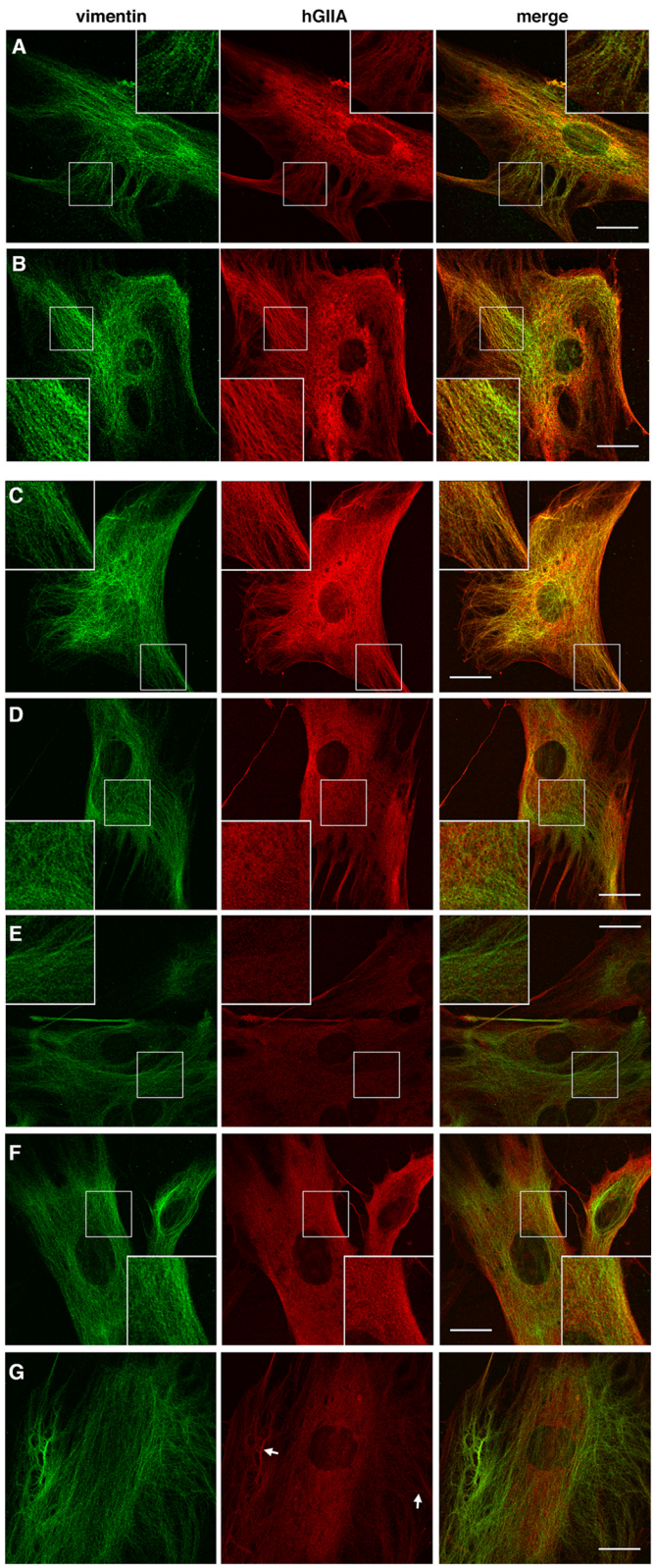

FIGURE 6. **Functionally selective inhibition of vimentin colocalization.** Immunofluorescence microscopy on RA61 FLSs treated with exogenous hGIIA alone (*A*) or hGIIA incubated with BPB (*B*). In a separate experiment RA61 FLSs were treated with exogenous hGIIA alone (*C*), hGIIA incubated with KH064 (*D*), hGIIA incubated with c2 (*E*), hGIIA incubated with cF (*F*), or hGIIA incubated with LY311727 (*G*). Staining and imaging of both hGIIA and vimentin was performed in all experiments as in Fig. 5 and described under "Experimental Procedures." *Columns 1–3* show vimentin (*green*), hGIIA (*red*), and a merge image, respectively. *Scale bars* represent 20 μm.

DISCUSSION

Recent studies have shown that hGIIA catalysis and signaling independently regulate arachidonic acid metabolism in cells depending on the biochemical context of the protein. For example, as shown here, hGIIA-dependent PGE_2 production and induction of COX-2 (9) in rheumatoid synovial cells is dependent solely on the signaling function of hGIIA. In contrast, the up-regulation of prostate cancer cell proliferation by exogenous hGIIA requires the catalytic function of hGIIA (37), as abrogation of catalytic activity with the H48Q mutation also abrogates the proliferative capacity of hGIIA. Our observation that these functions may be pharmacologically separated raises the possibility of development of potent and selective inhibitors of either catalysis or signaling that are active *in vivo* that might refine the specificity of the dual-function indole inhibitors tested thus far in the clinic. Current activity-selective inhibitors such as BPB are not subtype-specific in that they covalently modify histidines of several target proteins, and the structural studies presented here may aid in the design of more specific catalysis-selective inhibitors. In addition, of the 10 human $sPLA_2$ enzymes, 6 are known to bind to protein partners (38). The $sPLA_2$ enzymes have a highly conserved tertiary structure and catalytic site; however, they vary significantly in primary sequence (38), suggesting that development of functionally selective inhibitors may be possible and of benefit in dissecting out the mechanism of action of these enzymes in different biological contexts. Such inhibitors may also be useful in targeting rheumatoid arthritis, as *in vivo* animal model studies indicate that selective inhibition of hGIIA over other $sPLA_2$ enzymes is likely to be advantageous (39).

His-6 is unique to hGIIA in the family of $sPLA_2$ enzymes. In all structures of signaling active proteins (native, hGIIA-BPB, and the H48Q mutant), His-6 blocks substrate access to the active site cavity, suggesting that it must be displaced for substrate binding and catalysis to occur. This is indeed the case in the crystal structure of hGIIA bound to a transition state analog (28). Furthermore, in the hGIIA-transition state analog structure the His-6 is stabilized by a hydrogen bond between His-6 $N\delta^1$ and the $O\delta$ of Glu 17, which appears to be a hallmark of signaling inhibited hGIIA in rheumatoid FLS cells (Fig. 4*A*). Taken together, these data suggest that catalysis and signaling may be mutually exclusive and that His-6 may uniquely act as a switch in hGIIA between its signaling and catalytic modes of action.

These structures coupled with the pharmacological data on the inhibitors presented here raised the possibility that signaling inhibitors perturb the binding surface between vimentin and hGIIA, consistent with the observation that LY311727 is able to inhibit vimentin binding *in vitro* (36). Our immunofluorescence studies establish that exogenous hGIIA does indeed rapidly internalize in FLSs and very rapidly co-localizes with intracellular vimentin filaments. Importantly, abrogation of catalytic activity alone is insufficient to perturb hGIIA-vimentin colocalization. Furthermore, as predicted by the structural analysis, inhibitors that block hGIIA-mediated signaling, either selectively (c2 and cF) or non-selectively (LY311727 and KH064), also block hGIIA colocalization to vimentin.

These studies provide pharmacological and structural evidence for the interaction between vimentin and hGIIA having a role in the catalysis-independent function of hGIIA in rheumatoid FLSs that warrants further investigation. In the presence of a cytokine, the intracellular enzyme $cPLA_2$-α (cytosolic PLA_2-α, Group IVA PLA_2) is stimulated, resulting in arachidonic acid flux to COX-2. This together with the hGIIA-mediated increase in COX-2 protein leads to a significant up-regulation of prostaglandin production (9). Importantly, the studies imply that perturbation of this interaction is a plausible mechanism by which hGIIA-mediated eicosanoid production is blocked in these cells by both selective and non-selective signaling inhibitors. The structural data presented support such a mechanism, as inhibition of catalysis alone, without perturbing the known vimentin binding surface of hGIIA, is insufficient to block hGIIA-mediated eicosanoid production or to perturb the vimentin-hGIIA interaction. These findings identify the hGIIA-vimentin association as an important target for further study with respect to hGIIA function in regulating eicosanoid biosynthesis and raise important questions about the mechanism by which hGIIA colocalization could mediate up-regulation of COX-2.

The ability of these inhibitors to interfere with hGIIA signaling and to disrupt an interaction with vimentin provides the first evidence for a possible link between vimentin binding, hGIIA function, and arachidonic acid metabolism in synovial inflammation. Given the importance of hGIIA in mediating inflammation in models of arthritis (39), this mechanism also predicts a role for vimentin in arthritis pathology and identifies it as a potential target for drug development in this disease. In recent years vimentin has been shown to play a much wider role in cell function than its traditional role as an inert cellular scaffold (40). This study extends vimentin function to a lipid metabolic pathway important in the aberrant inflammatory response induced in immune-mediated pathological states in addition to an emerging functional role for vimentin in cancer progression.

The association between vimentin and hGIIA shown here identifies vimentin as an interesting target for further study in other diseases where a role for hGIIA has been established. This is particularly true in the case of tumorigenesis. Vimentin staining is frequently used as a marker for tumor identification and progression, is a signature marker, along with COX-2, of tumor dedifferentiation through the epithelial-mesenchymal transition that is a feature of cancer (41), and is increasingly being implicated functionally in cancer pathology (42). hGIIA is overexpressed in many cancers, and this expression has also been functionally implicated in mediating the pathology of certain types of cancer (43). This study suggests a potential mechanism whereby overexpression of hGIIA may potentiate this process that warrants further study.

When compared with small-molecule inhibitors that traditionally target catalytic sites, the manipulation of protein-protein interactions promises more versatility in the control of regulatory mechanisms. However, this approach is relatively uncharted for therapeutic agents. Targeting protein-protein interactions with small molecules is difficult as these interfaces generally lack well defined binding pockets. Although antibody

targeting of specific epitopes may be an effective means to inhibit the formation of protein complexes, these are generally expensive to produce and do not readily cross membrane bilayers. Thus, they are largely restricted to targeting extracellular epitopes (44). Furthermore, as the interface between two proteins is potentially much larger than can be covered by small molecules, an additional challenge is to target surfaces within these interfaces that will abrogate binding (45). In the case of LY311727 and KH064, the location of the active site cavity, central to the vimentin binding surface, provides a convenient and specific tether to target the hGIIA-vimentin interaction.

Acknowledgments—We thank the staff at beamline 14-BMC (BioCARS) at the Advanced Photon Source for support. Use of the Advanced Photon Source was supported by the United States Department of Energy, Basic Energy Sciences, Office of Science (Contract DE-AC02–06CH11357), and use of the BioCARS Sector 14 was supported by the National Institutes of Health, National Center for Research Resources (Grant RR007707) and the Australian Synchrotron Research Program.

REFERENCES

1. Yanes, O., Clark, J., Wong, D. M., Patti, G. J., Sánchez-Ruiz, A., Benton, H. P., Trauger, S. A., Desponts, C., Ding, S., and Siuzdak, G. (2010) Metabolic oxidation regulates embryonic stem cell differentiation. *Nat. Chem. Biol.* **6,** 411–417
2. Harizi, H., Corcuff, J.-B., and Gualde, N. (2008) Arachidonic-acid-derived eicosanoids. Roles in biology and immunopathology. *Trends Mol. Med.* **14,** 461–469
3. Funk, C. D. (2001) Prostaglandins and leukotrienes. Advances in eicosanoid biology. *Science* **294,** 1871–1875
4. Murakami, M., Taketomi, Y., Miki, Y., Sato, H., Hirabayashi, T., and Yamamoto, K. (2011) Recent progress in phospholipase A_2 research. From cells to animals to humans. *Prog. Lipid Res.* **50,** 152–192
5. Lambeau, G., and Gelb, M. H. (2008) Biochemistry and physiology of mammalian secreted phospholipases A_2. *Ann. Rev. Biochem.* **77,** 495–520
6. Zeiher, B. G., Steingrub, J., Laterre, P. F., Dmitrienko, A., Fukiishi, Y., Abraham, E., and EZZI Study Group (2005) LY315920NA/S-5920, a selective inhibitor of group IIA secretory phospholipase A2, fails to improve clinical outcome for patients with severe sepsis. *Crit. Care Med.* **33,** 1741–1748
7. Bradley, J. D., Dmitrienko, A. A., Kivitz, A. J., Gluck, O. S., Weaver, A. L., Wiesenhutter, C., Myers, S. L., and Sides, G. D. (2005) A randomized, double-blinded, placebo-controlled clinical trial of LY333013, a selective inhibitor of group II secretory phospholipase A_2, in the treatment of rheumatoid arthritis. *J. Rheumatol.* **32,** 417–423
8. Rosenson, R. S. (2010) Phospholipase A_2 inhibition and atherosclerotic vascular disease. Prospects for targeting secretory and lipoprotein-associated phospholipase A_2 enzymes. *Curr. Opin. Lipidol.* **21,** 473–480
9. Bryant, K. J., Bidgood, M. J., Lei, P.-W., Taberner, M., Salom, C., Kumar, V., Lee, L., Church, W. B., Courtenay, B., Smart, B. P., Gelb, M. H., Cahill, M. A., Graham, G. G., McNeil, H. P., and Scott, K. F. (2011) A bifunctional role for group IIA secreted phospholipase A_2 in human rheumatoid fibroblast-like synoviocyte arachidonic acid metabolism. *J. Biol. Chem.* **286,** 2492–2503
10. Bidgood, M. J., Jamal, O. S., Cunningham, A. M., Brooks, P. M., and Scott, K. F. (2000) Type IIA secretory phospholipase A_2 up-regulates cyclooxygenase-2 and amplifies cytokine-mediated prostaglandins production in human rheumatoid synoviocytes. *J. Immunol.* **165,** 2790–2797
11. Yokota, Y., Hanasaki, K., Ono, T., Nakazato, H., Kobayashi, T., and Arita, H. (1999) Suppression of murine endotoxic shock by $sPLA_2$ inhibitor, indoxam, through group IIA $sPLA_2$-independent mechanisms. *Biochim. Biophys. Acta* **1438,** 213–222
12. Singer, A. G., Ghomashchi, F., Le Calvez, C., Bollinger, J., Bezzine, S., Rouault, M., Sadilek, M., Nguyen, E., Lazdunski, M., Lambeau, G., and Gelb, M. H. (2002) Interfacial kinetic and binding properties of the complete set of human and mouse groups I, II, V, X, and XII secreted phospholipases A_2. *J. Biol. Chem.* **277,** 48535–48549
13. Reynolds, L. J., Hughes, L. L., and Dennis, E. A. (1992) Analysis of human synovial fluid phospholipase A_2 on short chain phosphatidylcholine-mixed micelles. Development of a spectrophotometric assay suitable for a microtiter plate reader. *Anal. Biochem.* **204,** 190–197
14. Arnett, F. C., Edworthy, S. M., Bloch, D. A., McShane, D. J., Fries, J. F., Cooper, N. S., Healey, L. A., Kaplan, S. R., Liang, M. H., Luthra, H. S. (1988) The American Rheumatism Association 1987 revised criteria for the classification of rheumatoid arthritis. *Arthritis Rheum.* **31,** 315–324
15. Otwinowski, Z., and Minor, W. (1997) in *Methods in Enzymology* (Carter, C. W. J., and Sweet, R. M., eds) pp. 307–326, Vol. 276, Academic Press, Elsevier, Amsterdam
16. Collaborative Computational Project, Number 4 (1994) The CCP4 suite. Programs for protein crystallography. *Acta Crystallogr. D Biol. Crystallogr.* **50,** 760–763
17. Emsley, P., and Cowtan, K. (2004) Coot. Model-building tools for molecular graphics. *Acta Crystallogr. D Biol. Crystallogr.* **60,** 2126–2132
18. Davis, I. W., Murray, L. W., Richardson, J. S., and Richardson, D. C. (2004) MOLPROBITY. Structure validation and all-atom contact analysis for nucleic acids and their complexes. *Nucleic Acids Res.* **32,** W615–W619
19. DeLano, W. L. (2002) The PyMOL Molecular Graphics System, DeLano Scientific, Palo Alto, CA
20. Smith, G. M., Ward, R. L., McGuigan, L., Rajkovic, I. A., and Scott, K. F. (1992) Measurement of human phospholipase A_2 in arthritis plasma using a newly developed sandwich ELISA. *Br. J. Rheumatol.* **31,** 175–178
21. Volwerk, J. J., Pieterson, W. A., and de Haas, G. H. (1974) Histidine at the active site of phospholipase A_2. *Biochemistry* **13,** 1446–1454
22. Church, W. B., Inglis, A. S., Tseng, A., Duell, R., Lei, P.-W., Bryant, K. J., and Scott, K. F. (2001) A novel approach to the design of inhibitors of human secreted phospholipase A_2 based on native peptide inhibition. *J. Biol. Chem.* **276,** 33156–33164
23. Tseng, A., Inglis, A. S., and Scott, K. F. (1996) Native peptide inhibition. Specific inhibition of type II phospholipases A_2 by synthetic peptides derived from the primary sequence. *J. Biol. Chem.* **271,** 23992–23998
24. Schevitz, R. W., Bach, N. J., Carlson, D. G., Chirgadze, N. Y., Clawson, D. K., Dillard, R. D., Draheim, S. E., Hartley, L. W., Jones, N. D., and Mihelich, E. D. (1995) Structure-based design of the first potent and selective inhibitor of human non-pancreatic secretory phospholipase A_2. *Nat. Struct. Biol.* **2,** 458–465
25. Hansford, K. A., Reid, R. C., Clark, C. I., Tyndall, J. D., Whitehouse, M. W., Guthrie, T., McGeary, R. P., Schafer, K., Martin, J. L., and Fairlie, D. P. (2003) D-Tyrosine as a chiral precursor to potent inhibitors of human nonpancreatic secretory phospholipase A_2 (IIa) with antiinflammatory activity. *Chembiochem.* **4,** 181–185
26. Wery, J. P., Schevitz, R. W., Clawson, D. K., Bobbitt, J. L., Dow, E. R., Gamboa, G., Goodson, T., Jr., Hermann, R. B., Kramer, R. M., and McClure, D. B. (1991) Structure of recombinant human rheumatoid arthritic synovial fluid phospholipase A_2 at 2.2A resolution. *Nature* **352,** 79–82
27. Lambeau, G., Ancian, P., Nicolas, J. P., Beiboer, S. H., Moinier, D., Verheij, H., and Lazdunski, M. (1995) Structural elements of secretory phospholipases A_2 involved in the binding to M-type receptors. *J. Biol. Chem.* **270,** 5534–5540
28. Scott, D. L., White, S. P., Browning, J. L., Rosa, J. J., Gelb, M. H., and Sigler, P. B. (1991) Structures of free and inhibited human secretory phospholipase A_2 from inflammatory exudate. *Science* **254,** 1007–1010
29. Renetseder, R., Dijkstra, B. W., Huizinga, K., Kalk, K. H., and Drenth, J. (1988) Crystal structure of bovine pancreatic phospholipase A_2 covalently inhibited by *p*-bromo-phenacyl-bromide. *J. Mol. Biol.* **200,** 181–188
30. Magro, A. J., Takeda, A. A., Soares, A. M., and Fontes, M. R. (2005) Structure of BthA-I complexed with *p*-bromophenacyl bromide. Possible correlations with lack of pharmacological activity. *Acta Crystallogr. D Biol. Crystallogr.* **61,** 1670–1677
31. Zhao, H., Tang, L., Wang, X., Zhou, Y., and Lin, Z. (1998) Structure of a snake venom phospholipase A_2 modified by *p*-bromo-phenacyl-bromide. *Toxicon* **36,** 875–886

32. Jain, M. K., Yu, B. Z., Rogers, J., Ranadive, G. N., and Berg, O. G. (1991) Interfacial catalysis by phospholipase A2. Dissociation constants for calcium, substrate, products, and competitive inhibitors. *Biochemistry* **30,** 7306–7317
33. Bayburt, T., Yu, B.-Z., Lin, H.-K., Browning, J., Jain, M. K., and Gelb, M. H. (1993) Human nonpancreatic secreted phospholipase A2. Interfacial parameters, substrate specificities, and competitive inhibitors. *Biochemistry* **32,** 573–582
34. Edwards, S. H., Thompson, D., Baker, S. F., Wood, S. P., and Wilton, D. C. (2002) The crystal structure of the H48Q active site mutant of human group IIA secreted phospholipase A_2 to 1.5 Å resolution provides an insight into the catalytic mechanism. *Biochemistry* **41,** 15468–15476
35. Koduri, R. S., Baker, S. F., Snitko, Y., Han, S. K., Cho, W., Wilton, D. C., and Gelb, M. H. (1998) Action of human group IIA secreted phospholipase A_2 on cell membranes. Vesicle but not heparinoid binding determines rate of fatty acid release by exogenously added enzyme. *J. Biol. Chem.* **273,** 32142–32153
36. Boilard, E., Bourgoin, S. G., Bernatchez, C., and Surette, M. E. (2003) Identification of an autoantigen on the surface of apoptotic human T cells as a new protein interacting with inflammatory group IIA phospholipase A_2. *Blood* **102,** 2901–2909
37. Sved, P., Scott, K. F., McLeod, D., King, N. J., Singh, J., Tsatralis, T., Nikolov, B., Boulas, J., Nallan, L., Gelb, M. H., Sajinovic, M., Graham, G. G., Russell, P. J., and Dong, Q. (2004) Oncogenic action of secreted phospholipase A_2 in prostate cancer. *Cancer Res.* **64,** 6934–6940
38. Scott, K. F., Graham, G. G., and Bryant, K. J. (2003) Secreted phospholipase A_2 enzymes as therapeutic targets. *Expert. Opin. Ther. Targets* **7,** 427–440
39. Boilard, E., Lai, Y., Larabee, K., Balestrieri, B., Ghomashchi, F., Fujioka, D., Gobezie, R., Coblyn, J. S., Weinblatt, M. E., Massarotti, E. M., Thornhill, T. S., Divangahi, M., Remold, H., Lambeau, G., Gelb, M. H., Arm, J. P., and Lee, D. M. (2010) A novel anti-inflammatory role for secretory phospholipase A_2 in immune complex-mediated arthritis. *EMBO Mol. Med.* **2,** 172–187
40. Eriksson, J. E., Dechat, T., Grin, B., Helfand, B., Mendez, M., Pallari, H. M., and Goldman, R. D. (2009) Introducing intermediate filaments. From discovery to disease. *J. Clin. Invest.* **119,** 1763–1771
41. Thiery, J. P., Acloque, H., Huang, R. Y., and Nieto, M. A. (2009) Epithelial-mesenchymal transitions in development and disease. *Cell* **139,** 871–890
42. Lahat, G., Zhu, Q. S., Huang, K. L., Wang, S., Bolshakov, S., Liu, J., Torres, K., Langley, R. R., Lazar, A. J., Hung, M. C., and Lev, D. (2010) Vimentin is a novel anti-cancer therapeutic target. Insights from *in vitro* and *in vivo* mice xenograft studies. *PLoS One* **5,** e10105
43. Scott, K. F., Sajinovic, M., Hein, J., Nixdorf, S., Galettis, P., Liauw, W., de Souza, P., Dong, Q., Graham, G. G., and Russell, P. J. (2010) Emerging roles for phospholipase A_2 enzymes in cancer. *Biochimie* **92,** 601–610
44. Gadek, T. R., and Nicholas, J. B. (2003) Small molecule antagonists of proteins. *Biochem. Pharmacol.* **65,** 1–8
45. Arkin, M. R., and Wells, J. A. (2004) Small-molecule inhibitors of protein-protein interactions. Progressing towards the dream. *Nat. Rev. Drug Discov.* **3,** 301–317

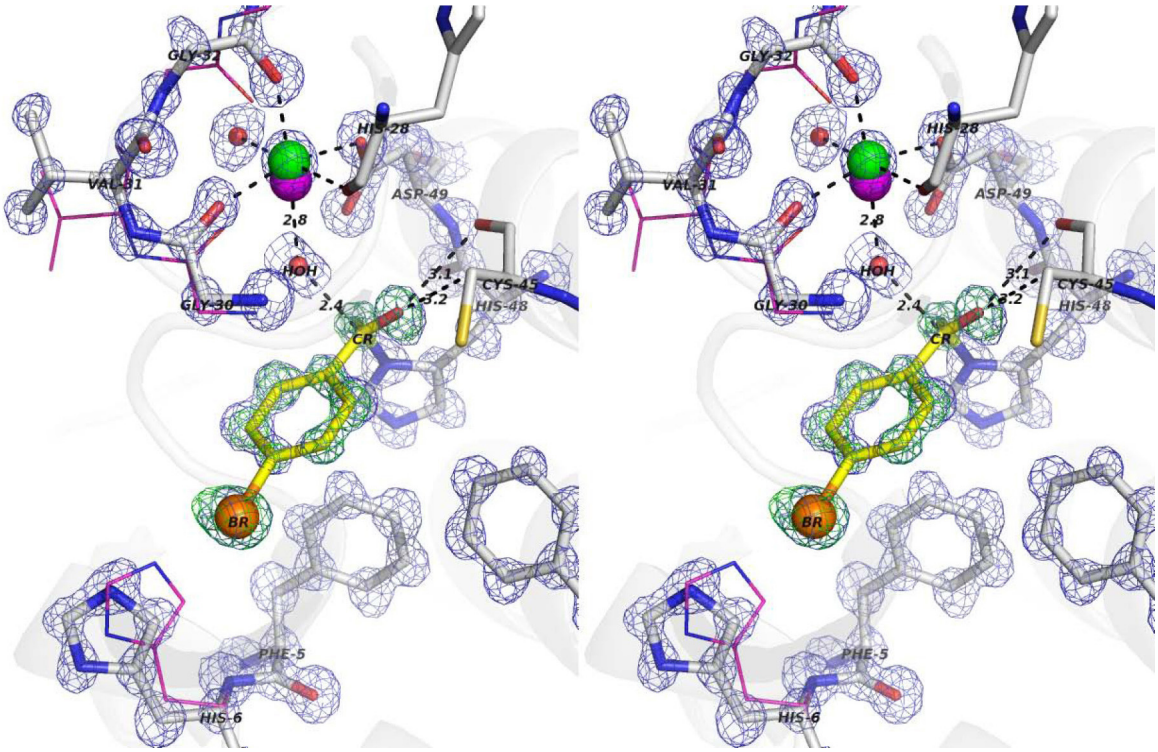

Supplemental Figure 1. Stereo image of BPB in the active site of hGIIA.
BPB is displayed in yellow stick format, covalently bound to the active site residue His 48. 2fo-1fc electron density contoured at 1.5 σ is displayed in blue mesh and unbiased 1fo-1fc density contoured at 5.0 σ and generated before the inhibitor was included in rounds of refinement is displayed in green mesh. The 6 oxygen atoms coordinating the active site calcium are displayed with dashed lines to highlight their interaction with calcium. Apparent steric clashes are also highlighted with dashed lines and the distances labelled in Å units. HOH is also shown to be interacting with the carbonyl carbon (CR) on BPB. The active site calcium of the hGIIA-BPB complex is displayed in green. Residues directly interacting with BPB are shown in stick format as well as the calcium-binding loop from residues Gly30 to Arg34 and the equivalent residues from the structure of native hGIIA are shown as lines in magenta. The active site calcium of hGIIA-BPB and the native enzyme are displayed green and magenta spheres respectively.

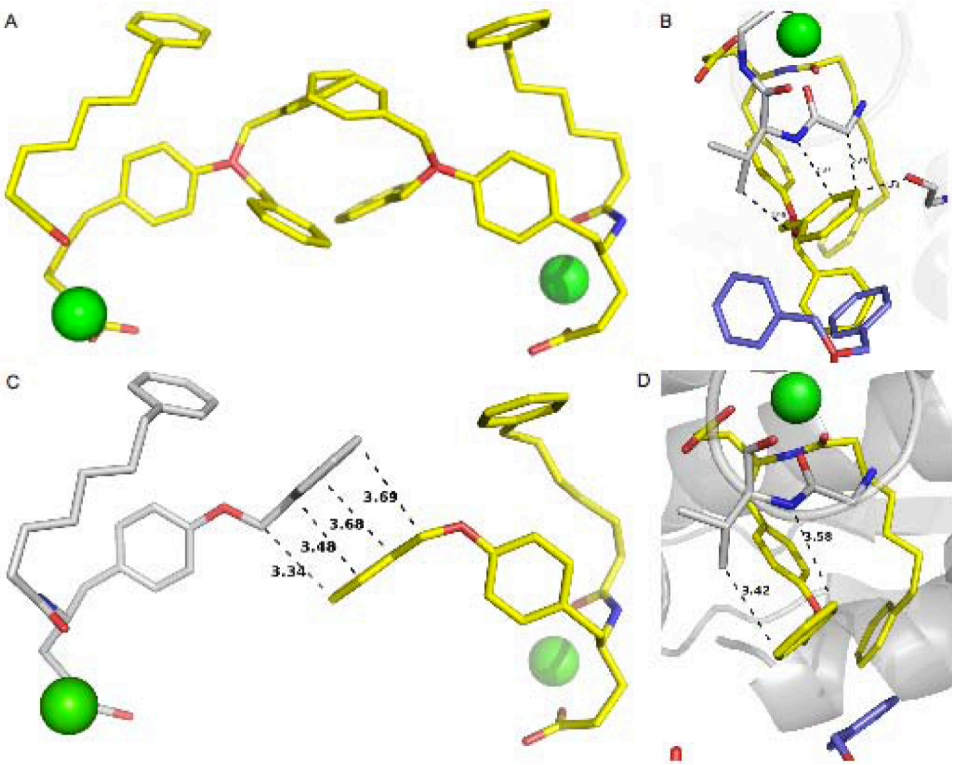

Supplemental Figure 2. Comparison between current and previously published hGIIA-KH064 (PDB accession code:1j1a) structures.
(A) and (B) were rendered from 1j1a and the equivalent view of the current hGIIA-KH064 structure presented in this manuscript are shown in (C) and (D). Multiple conformations of KH064 in 1j1a (A) contrast to two well-defined distinct conformations in the current structure (C). Clashes between KH064 and the calcium-binding loop in 1j1a are highlighted in (B) with dashed lines with distances marked. The equivalent interactions in the current structure are highlighted in (D).

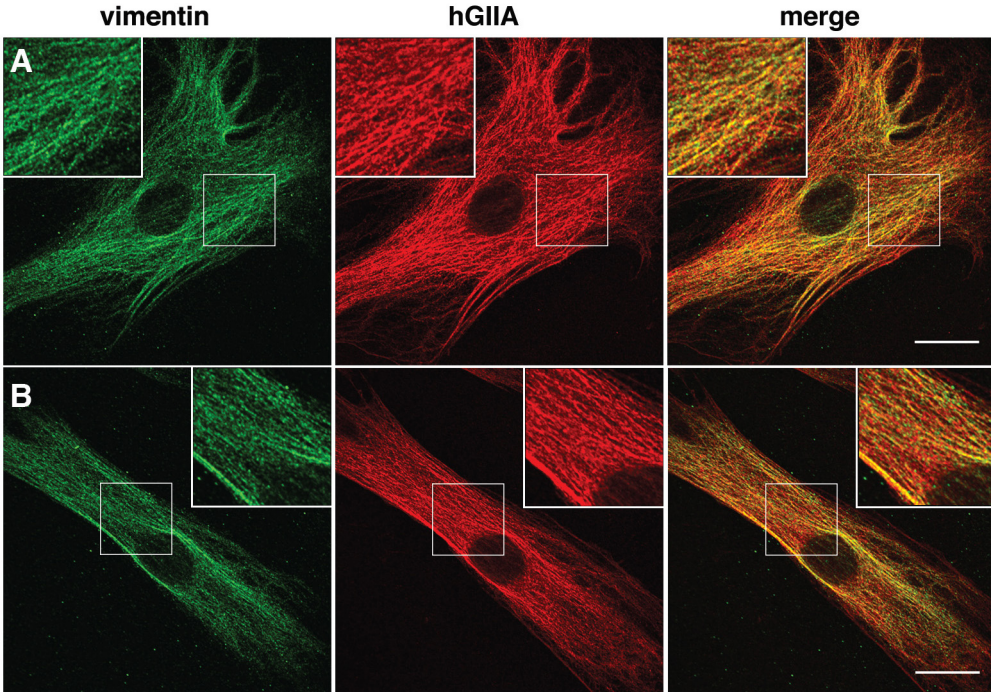

Supplemental Figure 3. hGIIA internalizes rapidly and co-localizes with vimentin. (A-B) Additional examples of immunofluorescence microscopy results on RA61 FLSs treated with exogenous hGIIA and stained for hGIIA and vimentin as in Figure 5D.

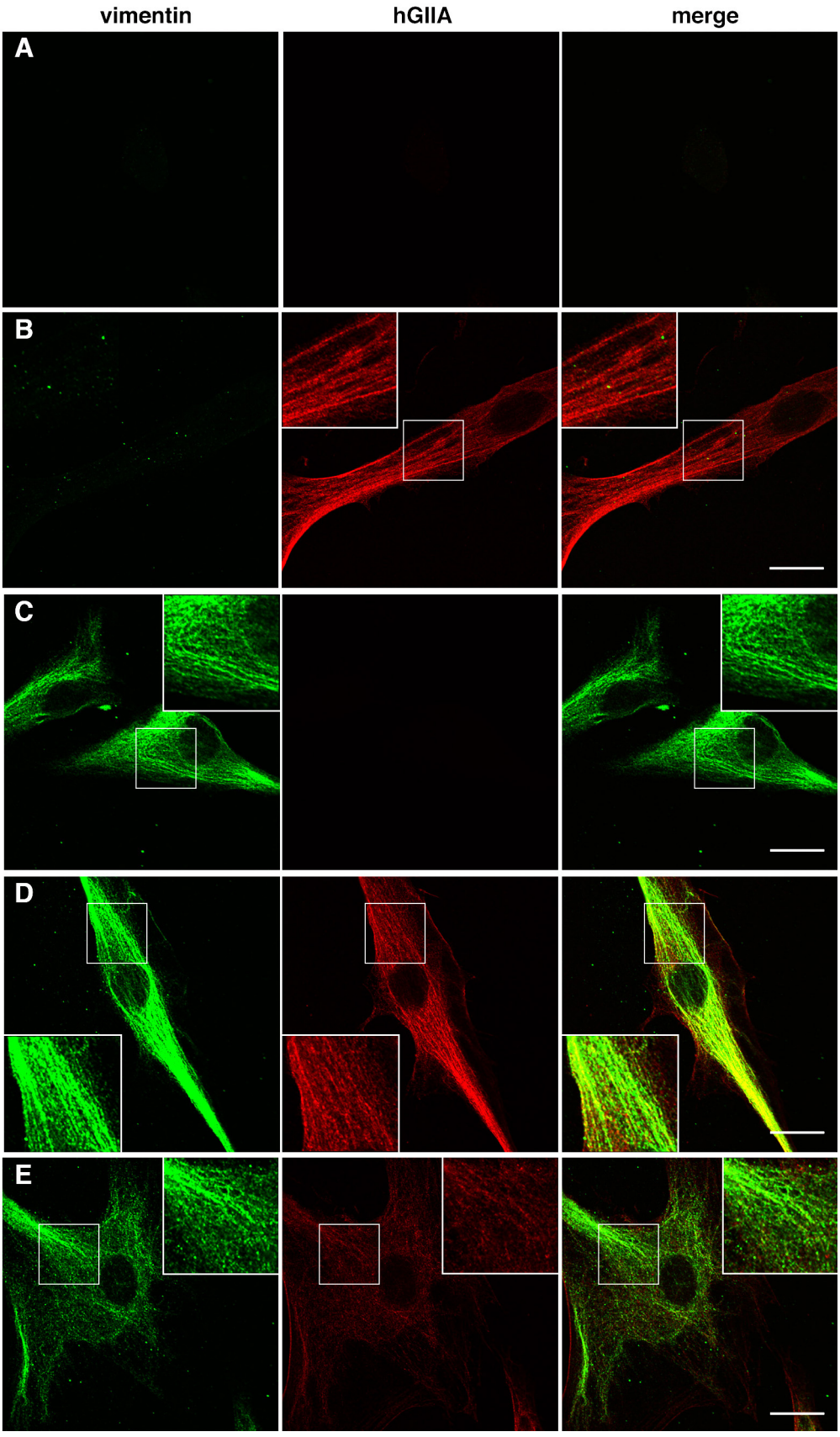
vimentin
hGIIA
merge
A
B
C
D
E

Supplemental Figure 4. hGIIA internalizes rapidly and co-localizes with vimentin. Immunofluorescence microscopy on cells stained for hGIIA in the absence of hGIIA treatment (A). Exogenous hGIIA was applied and cells were stained for hGIIA in (B), vimentin (C) or hGIIA and vimentin in (D-E). Cells were RA**57** human rheumatoid FLSs. Columns 1-3 show vimentin (green), hGIIA (red) and a merge image, respectively. Scale bars represent 20 μm.

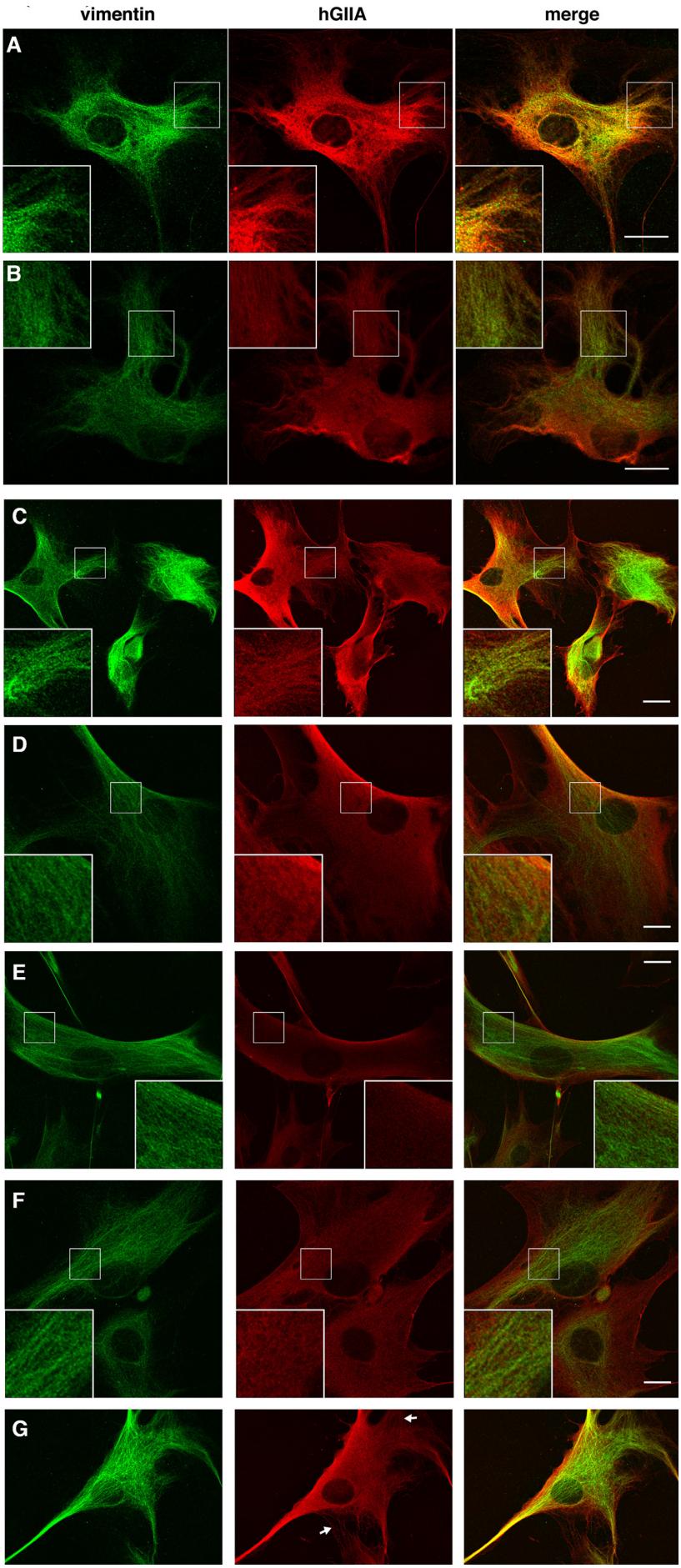
vimentin
hGIIA
merge
A
B
C
D
E
F
G

Supplemental Figure 5. Functionally selective inhibition of vimentin binding.
Immunofluorescence microscopy on RA57 FLSs treated with (A) exogenous hGIIA alone or (B) hGIIA incubated with BPB. In a separate experiment, RA57 FLSs were treated with (C) exogenous hGIIA alone, (D) hGIIA incubated with KH064, (E) hGIIA incubated with c2, (F) hGIIA incubated with cF or (G) hGIIA incubated with LY311727. Staining of both hGIIA and vimentin was performed in all experiments. Columns 1-3 show vimentin (green), hGIIA (red) and a merge image, respectively. Scale bars represent 20 μm.

Selective Inhibition of Human Group IIA-secreted Phospholipase A_2 (hGIIA) Signaling Reveals Arachidonic Acid Metabolism Is Associated with Colocalization of hGIIA to Vimentin in Rheumatoid Synoviocytes

Lawrence K. Lee, Katherine J. Bryant, Romaric Bouveret, Pei-Wen Lei, Anthony P. Duff, Stephen J. Harrop, Edwin P. Huang, Richard P. Harvey, Michael H. Gelb, Peter P. Gray, Paul M. Curmi, Anne M. Cunningham, W. Bret Church and Kieran F. Scott

J. Biol. Chem. 2013, 288:15269-15279.
doi: 10.1074/jbc.M112.397893 originally published online March 12, 2013
